Applied and Computational Mechanics 15 (2021) 5–18

Influence of input parameters in radial compressor design algorithm on the efficiency and its sensitivity analysis

P. Kovář[a,*], T. Kaňka[a], P. Mačák[a], A. Tater[a], T. Vampola[a]

[a] Department of Instrumentation and Control Engineering, Faculty of Mechanical Engineering, Center of Advanced Aerospace Technology, Czech Technical University in Prague, Technicka 4, 166 07, Prague 6, Czech Republic

Received 27 October 2020; accepted 1 April 2021

Abstract

Nowadays there are lots of methods using three-dimensional or quasi three-dimensional CFD analysis. Unfortunately, this approach is still very demanding, so that quick preliminary design algorithms have still its importance, even though simplified analytical model of radial compressor gives less accurate results. Obtained results can be used in later stages of the radial compressor (RC) design, such as definition of spatial impeller geometry and CFD computation. The article presents the influence of input parameters in the radial compressor design algorithm on the efficiency. The assembled mathematical model of RC is derived from the basic laws of continuum mechanics and can be used for a quick assessment of the preliminary design concept of the RC. A sensitivity analysis is performed on input parameters to select parameters that have the dominant effect on the monitored performance indicators. On the basis of the sensitivity analysis, a multicriteria optimization process was assembled to increase the performance parameters.

Keywords: radial compressor, design algorithm, sensitivity study, optimization

1. Introduction

Compressors are a key component in an aircraft engine and they can be divided into two groups based on the direction of the airflow leaving the rotor. Both types of compressors are commonly used in the aircraft industry. Centrifugal compressors are mostly used in smaller aircraft engines, especially in turbo shaft and subsidiary engines [8]. Radial compressor is the most efficient and compact compression device for the flow range 0.3–95 $\mathrm{m}^3\,\mathrm{s}^{-1}$ [19].

Airflow entering the centrifugal compressor in axial direction is turned into radial direction along the impeller. Impeller delivers the kinetic energy into the airflow. Vane and vaneless diffusers convert kinetic energy of the air into pressure energy. Lastly, collector redirects the airflow back into axial direction and provides a connection following stages of aircraft engine.

Designing a state of the art centrifugal compressor requires a significant amount of engineering effort. Airflow inside the radial compressor is a complex 3D phenomenon. However, the importance of a preliminary compressor design cannot be omitted [11, 20]. Initial calculations regarding radial-flow compressor stage may be obtained via one-dimensional computation along the mean streamline. There is a large number of 1D design algorithms.

Růžek and Kmoch in [14] applied fundamental laws of thermodynamics on radial compressor for aircraft applications. For the needs of 1D design, effort to quantify properties of a complex airflow in RC via several engineering constants is spent. This leads to a relatively simple and fast 1D design algorithm, which is able to calculate fundamental compressor parameters.

*Corresponding author. Tel.: +420 224 359 772, e-mail: Patrik.Kovar@fs.cvut.cz.
https://doi.org/10.24132/acm.2021.653

Vaněk and Matoušek in [17] presented an algorithm used for radial compressor design, namely impeller and diffuser. The need of one-dimensional design preceding the design of complex spatial geometry is emphasized.

Zurita-Ugalde in [21] presented design algorithm for stationary industrial radial compressor. Even though this paper does not deal with aerial turbomachinery, significant resemblance with [14] and [17] can be seen. Described approach is based on flow path mean-line design using circular arc presented by Smith in [16].

Xu in [19] and [20] described basic considerations which can be used for guiding industry centrifugal compressor design. Presented recommendations are based on author's experience. Preliminary design then can be done using herein presented diagrams.

Computation based on characteristics of known measured compressors is presented by Fözö in [8]. Design approach is then based on similarity and dimensionless parameters.

Shiff presented a complex tool for centrifugal compressor stage in [15]. In comparison with above mentioned algorithms, Shiff's method does require less input parameters. The computation is based on Aungier's calculation procedure described in [1] and [2].

It is possible to obtain the same performance of the centrifugal compressor with different computed geometries [20]. Since the basic thermodynamic and geometric design is included in the initial 1D design, the spatial geometry of the impeller blades may be computed. If the design requirements are not satisfied, the design returns back to its former phase [11].

Nowadays there are lots of methods using three-dimensional or quasi three-dimensional CFD analysis [5, 13]. Unfortunately, this approach is still very demanding, so that quick preliminary design algorithms have still its importance, even though simplified analytical model of radial compressor gives less accurate results. Obtained results can be iteratively refined. Output of one-dimensional design is later used to determine spatial configuration of the radial compressor. Defined geometry can be subsequently tested and modified in chosen CFD software.

Presented one-dimensional design algorithm is based on [14] and [17]. Verified analytical models are combined and extended by several features, such as optimization of inlet axial velocity. Applying pre-whirl is also possible. Mean-line, hub and shroud lines are created using Bézier polynomials. Similar approach is described in [3]. Furthermore, sensitivity study is performed to evaluate the effect of input parameters on the performance of the radial compressor. Finally, results from parametric study are used in optimization tool. Optimization outlines the dependency of calculated results on design requirements.

2. Design algorithm

For the preliminary radial compressor design, one-dimensional methods are often used. Presented algorithm is mainly designed to compute both thermodynamic quantities at individual cross-sections and the basic geometry of the centrifugal compressor, that can be seen in Fig. 1. Obtained results may be used in more demanding three-dimensional methods. Two design approaches are possible. Radial compressor can be designed either at its strength limit (characterized by $u_{2\,\mathrm{max}}$[1]) or with respect to a specified total pressure ratio π_{ct} and efficiency η_{ct}. Even though the second approach is more common in the industry, the first design approach is preferred in this paper to examine the capabilities of the presented design algorithm.

[1]The strength of the impeller blade material can be characterized by maximal circumferential velocity at the impeller outlet. Magnitude of $u_{2\,\mathrm{max}}$ varies in range of 380–550 $\mathrm{m\,s^{-1}}$ [4].

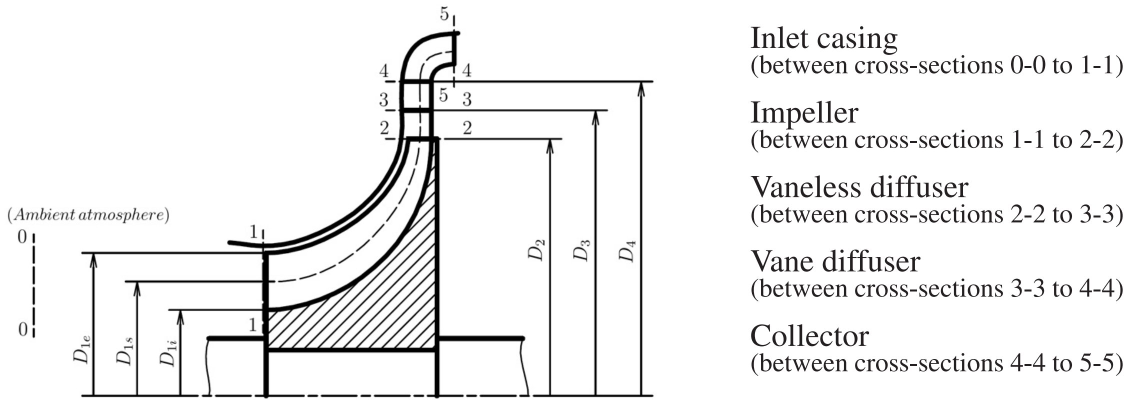

Fig. 1. Radial compressor sketch

2.1. Design procedure

Main design input parameters like total pressure ratio π_{ct}, mass flow Q_v, rotational speed n, impeller inlet hub diameter D_{1i}, maximal external diameter of radial compressor $D_{5e\,\max}$ and flight velocity c_0 depend on the general engine design. Static pressure p_0 and static temperature T_0 are computed from design altitude H via ISA model. Atmospheric total pressure p_{0t} and temperature T_{0t} are then computed using the equations of gas dynamics

$$p_{0c} = p_0 \left(1 + \frac{\kappa - 1}{2} M_0^2\right)^{\frac{\kappa}{\kappa-1}}, \quad T_{0c} = T_0 \left(1 + \frac{\kappa - 1}{2} M_0^2\right), \tag{1}$$

where M_0 is the Mach number at the compressor inlet and κ is the specific heat ratio. The last of main parameters is collector outlet airflow velocity c_5 that is determined according to the needs of the following engine component (100–120 $\mathrm{m\,s^{-1}}$ if combustion chamber is considered [14]).

Impeller is the only component of radial compressor which delivers kinetic energy into the airflow. Both pressure and temperature increase in this section. At the impeller inlet there has to be defined absolute inlet velocity. It has two components – axial component c_{1a} (100–150 $\mathrm{m\,s^{-1}}$ [14]) and circumferential component c_{1u} (0–50 $\mathrm{m\,s^{-1}}$ [14]). Motion of an air particle is described by Euler's equation enhanced with friction loss [14]

$$\frac{\mathrm{d}\boldsymbol{c}}{\mathrm{d}t} = -\frac{1}{\rho}\nabla p + \boldsymbol{F_e} - \boldsymbol{F_f}. \tag{2}$$

For rotational motion, equation (2) can be written as [14]

$$\frac{\mathrm{d}\boldsymbol{w}}{\mathrm{d}t} - \omega^2 \boldsymbol{r} + 2\boldsymbol{\omega} \times \boldsymbol{w} + \frac{1}{\rho}\nabla p = 0. \tag{3}$$

By simplifying (3), the equations describing an impeller with infinite number of blades are derived. Due to a finite number of blades and inertial force influencing air particles, a recirculation of air in individual airflow channels is caused. As a result, circumferential component of absolute velocity at the impeller outlet c_{2u} is different for the impeller with finite and infinite number of blades ($c_{2u} \neq c_{2u\infty}$). This phenomenon is quantified by slip coefficient μ defined as

$$\mu = \frac{c_{2u}}{c_{2u\infty}}. \tag{4}$$

Work input into air flow can be expressed [14] as

$$w_{ek} = u_2 c_{2u} - u_{1s} c_{1us} + w_r, \tag{5}$$

where w_r represents aerodynamical and frictional losses along the impeller. Absolute circumferential velocity at the impeller outlet c_{2u} can be written as

$$c_{2u} = \mu(u_2 - c_{2r} \cot \varphi_2), \tag{6}$$

where c_{2r} is an absolute radial velocity at the impeller outlet and φ_2 stands for angle of blades at the impeller outlet.

The value of μ can be estimated by several semi-empirical equations. Each of these equations works for a specific group of radial compressors. For aircraft radial compressor with a number of impeller blades around 30, equation (7) derived by Eckert [6] is used

$$\mu = \frac{1}{1 + \frac{\pi \sin^2 \varphi_2}{2 z_I \left(1 - \frac{D_{1s}}{D_2}\right)}}, \tag{7}$$

where angle of blades φ_2 is chosen in span $45°$–$90°$ [4]. The number of impeller blades z_I is customizable. The empirical equation from [14] is used to estimate the upper and lower bound of z_I in presented algorithm as

$$z_I = \frac{2\pi \sin \frac{\varphi_1 + \varphi_2}{2}}{K \ln \frac{D_2}{D_{1e}}}, \text{ where } K = \langle 0.35; 0.45 \rangle. \tag{8}$$

The number of impeller blades is often more than twenty-two in aircraft engines [14]. Other important parameters defining impeller geometry are average blade thickness at the impeller outlet t_{2s} and radial clearance δ_m. The unfavorable effects caused by radial clearance are described in [4] and [20]. Additional parameters describing the impeller geometry can be seen in Fig. 2.

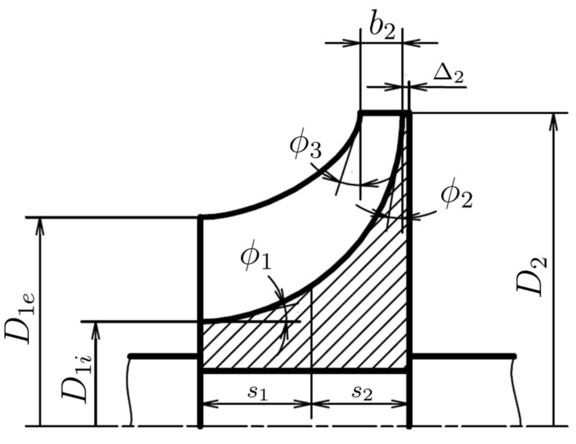

$$\frac{\Delta_2}{D_2} = \langle 0.0075; 0.01 \rangle$$
$$\frac{s_1}{D_2} = \langle 0.15; 0.2 \rangle$$
$$\frac{s_2}{D_2} = \langle 0.1; 0.15 \rangle$$
$$\phi_1 = \langle 10; 20 \rangle°$$
$$\phi_2 = \langle 0; 7 \rangle°$$
$$\phi_3 = \langle 5; 15 \rangle°$$

Fig. 2. Impeller geometry, recommended spans are taken from [14]

Presence of shock waves is undesirable since the transition to supersonic airflow causes additional aerodynamic losses. Impeller rotation induces circumferential velocity with specific magnitude proportional to the radial distance from axis of rotation. Relative velocity at the impeller tip w_{1e} affects the properties of airflow along the impeller. Thus, it is required that

$$M_{w1e} = \frac{w_{1e}}{\sqrt{\kappa r T_1}} < 1. \tag{9}$$

The magnitude of w_{1e} is obtained from the components of absolute inlet velocity c_{1a} and c_{1u} and circumferential velocity at the impeller inlet tip u_{1e} as

$$w_{1e} = \sqrt{c_{1a}^2 + (u_{1e} - c_{1u})^2}. \tag{10}$$

From (10), it can be seen that there are two ways of reducing M_{w1e}. Since u_{1e} is proportional to the rotational speed n which directly influences the pressure ratio π_{ct}, the modification of c_{1a} and c_{1u} comes to mind. That is why the optimization of c_{1a} can be applied. If necessary, pre-whirl blading to increase c_{1u} may be designed, as well.

Density of air at the impeller outlet ρ_2 is necessary to determine the geometry of the impeller outlet, thus, an iterative calculation is used. The value of ρ_2 is unknown in the first iteration and the width of the airflow channel at impeller outlet b_2 is calculated. After that, impeller velocity field and aerodynamic losses are computed. Consequently, the temperature (and pressure) of air at the impeller outlet T_2 (p_2) are evaluated. Finally, new value of ρ_2 is determined. Iterative process is terminated when a convergence condition is reached. The impeller isotropic efficiency η_{Iis} is calculated as

$$\eta_{Iis} = \frac{\pi_{It}^{\frac{\kappa-1}{\kappa}} - 1}{\Delta T_t}, \text{ where } \Delta T_t = \frac{T_{2t} - T_{1t}}{T_{1t}}. \tag{11}$$

When the dimensions of the impeller and the properties of air leaving the impeller are calculated, a diffuser can be designed. It transforms kinetic energy into pressure energy. Diffuser is divided into vane and vaneless part. Vane diffuser design assumes subsonic airflow, thus vaneless diffuser is placed after impeller outlet and following assumptions are taken into account

$$D_2' = D_2, \quad b_2' = b_2, \quad \rho_2' = \rho_2, \quad c_{2u}' = c_{2u}, \quad T_{3c} = T_{2c}, \quad b_3 = b_2', \quad \gamma = 0,$$

where the superscript “′” refers to the vaneless diffuser inlet. Vaneless diffuser ensures absence of shock waves even though airflow leaving impeller is supersonic. Shock waves appear unless radial component of velocity at impeller outlet c_{2r} is subsonic ($M_{c2r} < 1$). Length of vaneless diffuser is calculated with respect to given Mach number at the vane diffuser inlet M_3 [14] as

$$D_3 = D_2 \frac{b_2 \sin\alpha_2' \, M_2'}{b_3 \sin\alpha_3 \, M_3} \left(\frac{1 + \frac{\kappa-1}{2} M_3^2}{1 + \frac{\kappa-1}{2} M_2'^2} \right)^{\frac{n_2+1}{2(n_2-1)}}, \tag{12}$$

where

$$\alpha_3 = \arctan\left(\frac{b_2}{b_3} \tan\alpha_2' \left(\frac{M_2'}{M_3} \right)^{\frac{n_2-\kappa}{\kappa(n_2-1)}} \left(\frac{1 + \frac{\kappa-1}{2} M_3^2}{1 + \frac{\kappa-1}{2} M_2'^2} \right)^{\frac{n_2+\kappa}{2\kappa(n_2-1)}} \right) \tag{13}$$

and n_2 is determined from

$$\frac{n_2}{n_2 - 1} = \frac{\kappa}{\kappa - 1} \; \frac{4 \sin\alpha_2' \, (\overline{b_2'} + \tan\gamma \, \sin^2\alpha_2' - \xi_D \sin^2\alpha_2')}{4 \sin\alpha_2' \, (\overline{b_2'} + \tan\gamma \, \sin^2\alpha_2') - \xi_D (M_2' \sin^2\alpha_2' - \cos^2\alpha_2')}. \tag{14}$$

Since the vane diffuser has higher efficiency over the vaneless diffuser [14], the remaining velocity reduction is performed in the vane diffuser. Number of vanes in the vane diffuser z_D is customizable as well as z_I and according to [14] it is often chosen in the range $15 - 35$. Other input parameters are Laval number at the vane diffuser outlet λ_4 and polytropic index n_D. Diffuser geometric configuration of a single vane can be seen in Fig. 3.

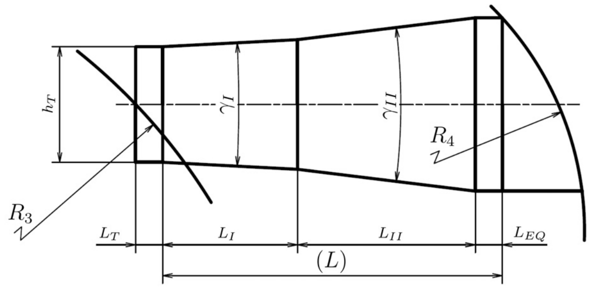

$$\frac{L_T}{h_T} = \langle 0.4; 0.7 \rangle$$
$$\frac{L_I}{h_T} = \langle 3.5; 4 \rangle$$
$$\frac{L_{II}}{h_T} = \langle 3; 4.5 \rangle$$
$$\frac{L_{EQ}}{h_T} = \langle 0; 2 \rangle$$
$$\gamma_I = \langle 4; 6 \rangle^\circ$$
$$\gamma_{II} = \langle 9; 11 \rangle^\circ$$

Fig. 3. Diffuser vane geometry, recommended spans are taken from [14]

Coefficients describing losses take into account influences of boundary layer at the individual component ϵ_i, pressure losses marked as σ_i and friction losses ξ_i. Ranges for coefficients ϵ_i are derived from basic considerations about boundary layer. Pressure loss coefficients and friction loss coefficient at impeller ξ_I are taken from [14]. Range of friction loss coefficient at vaneless diffuser ξ_I is based on measurement developed by Johnson and Dean in [10]. Recommended spans of these loss coefficients are presented in Table 1.

The flowchart of the presented algorithm workflow is visualized in Fig. 4.

Table 1. Loss coefficients summary

Section	Impeller				Vaneless diff.	Vane diff.			Collector	
Parameter	ϵ_1	ϵ_2	σ_I	ξ_I	ξ_D	ϵ_3	ϵ_4	σ_D	ϵ_5	σ_C
Span	$\langle 0.9; 1 \rangle$	$\langle 0.9; 1 \rangle$	$\langle 0.97; 0.99 \rangle$	$\langle 0.24; 0.4 \rangle$	$\langle 0.03; 0.04 \rangle$	$\langle 0.9; 1 \rangle$	$\langle 0.9; 1 \rangle$	$\langle 0.96; 1 \rangle$	$\langle 0.9; 1 \rangle$	$\langle 0.97; 0.98 \rangle$

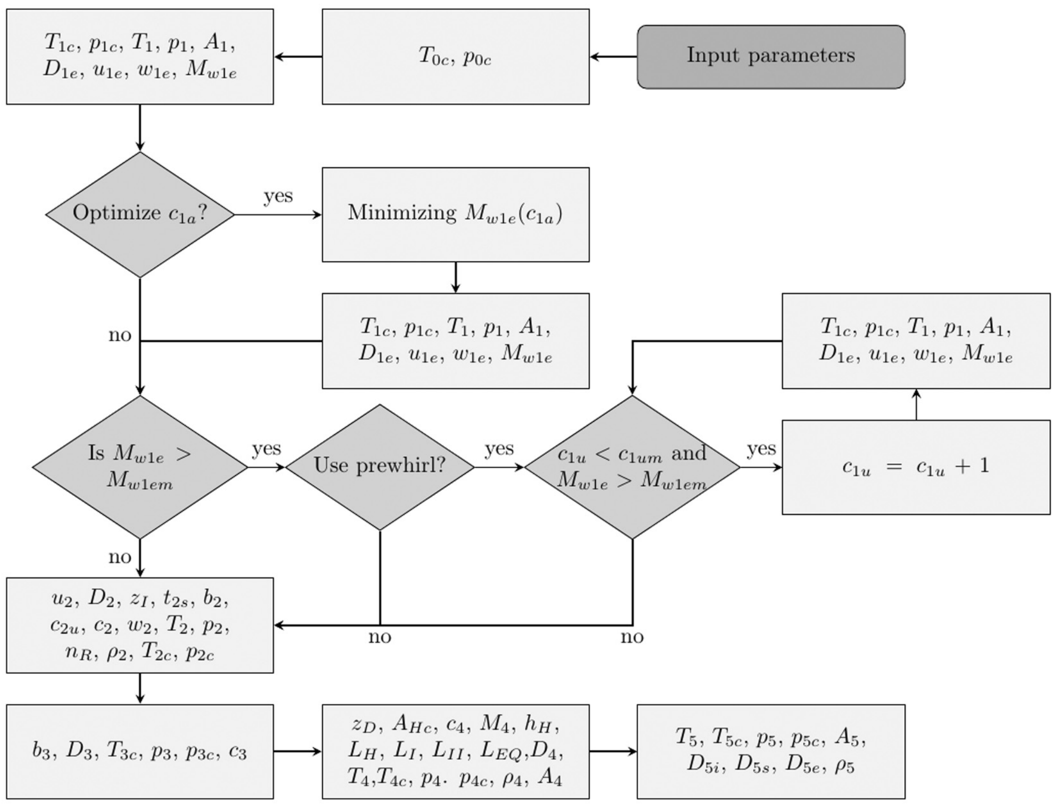

Fig. 4. Flowchart of the design algorithm

3. Comparison with another design algorithm

Compressor designs comparison with design algorithm described in [14] is presented in this section. Since the design algorithm presented in this paper is derived from methods used in [14] and [17], several input parameters used in [14] differ from those in the presented algorithm. That is the reason why particular results in [14] (rotational speed n, impeller inlet hub diameter D_{1i}, number of impeller blades n_I, etc.) were used as input parameters in the presented algorithm.

Methodology used in [14] does not include impeller and vane diffuser geometry[2]. Overview of the input parameters used for verification is ordered in Table 2. Parameters common in both algorithms are marked with a symbol '*'.

Table 2. Input parameters

Parameter	Q_v*	n	D_{1i}	$D_{5e\,\max}$	c_0*	c_5*	p_0*	T_0*
Unit	$[\mathrm{kg\,s^{-1}}]$	[RPM]	[mm]	[mm]	$[\mathrm{m\,s^{-1}}]$	$[\mathrm{m\,s^{-1}}]$	[kPa]	[K]
Value	12	15 500	124	900	0	120	101	288
Parameter	$u_{2\,\max}$	$\pi*$	$\eta*$	c_{1a}	$c_{1u}*$	φ_2*	δ_m*	σ_E*
Unit	$[\mathrm{m\,s^{-1}}]$	[1]	[1]	$[\mathrm{m\,s^{-1}}]$	$[\mathrm{m\,s^{-1}}]$	$[^\circ]$	[mm]	[1]
Value	500	4.24	0.79	124	0	90	0.5	0.98
Parameter	ξ_I	M_3*	ξ_D*	λ_4	n_D	σ_D	K_{b4}	σ_C
Unit	[1]	[1]	[1]	[1]	[1]	[1]	[1]	[1]
Value	0.33	0.88	0.03	0.31	1.65	0.98	1	0.98

Computed results are compared in Table 3. The main design parameters π_{ct}, η_{cis}, D_{5e} correspond with the results in [14]. Requirement on Mach number at the impeller tip, described by (9), was satisfied. Impeller dimensions D_{1e}, D_2 and request on its "strength" expressed with $u_{2\,\max}$ are very similar. Higher difference in pressure at the cross-section 2-2 is caused by considering a different loss model than the author [14] used. On the other hand, the presented design algorithm assumes more losses in the diffusers and collector, so that thermodynamic quantities at the compressor outlet differ a little.

Table 3. 1D design algorithm validation – outputs

Parameter	π_{kc}	η_{kc}	D_{5e}	D_{1e}	M_{w1e}	u_2	μ	D_2
Unit	[1]	[1]	[mm]	[mm]	[1]	$[\mathrm{m\,s^{-1}}]$	[1]	[mm]
Example from [14]	4.18	0.79	809	354	0.93	442	0.91	545
Presented algorithm	4.24	0.79	826	357	0.94	441	0.9	547
Difference [%]	$+1.44$	0	$+2.06$	$+0.84$	$+1.06$	-0.23	-1.11	$+0.37$
Parameter	p_{2c}	p_2	T_{2c}	T_2	p_{5c}	p_5	T_{5c}	T_5
Unit	[kPa]	[kPa]	[K]	[K]	[kPa]	[kPa]	[K]	[K]
Example from [14]	475	230	473	385	415	394	473	465
Presented algorithm	507	251	479	392	421	396	479	472
Difference [%]	$+6.31$	$+8.37$	$+1.25$	$+1.79$	$+1.43$	$+0.51$	$+1.25$	$+1.48$

[2]Parameters in Fig. 3 are estimated to meet designed vane diffuser outlet diameter D_4 in [14]

4. Sensitivity study

There are 27 input coefficients entering the presented algorithm. Significant effort has been spent to determine the rate of change in the designed pressure ratio π_{ct} and the isentropic efficiency η_{cis} caused by the varying of individual input parameters.

Due to a computational difficulty, a variation of one parameter was performed while others were fixed at their span centres. We gained an overview of the influence of individual parameters on the 1D radial-flow compressor design. The sensitivities of chosen parameters are plotted in Fig. 5. We can see that the design fundamentally depends on the choice of the $u_{2\,\max}$ parameter, whereas the inlet casing pressure loss coefficent σ_E affects the design to a very little extent.

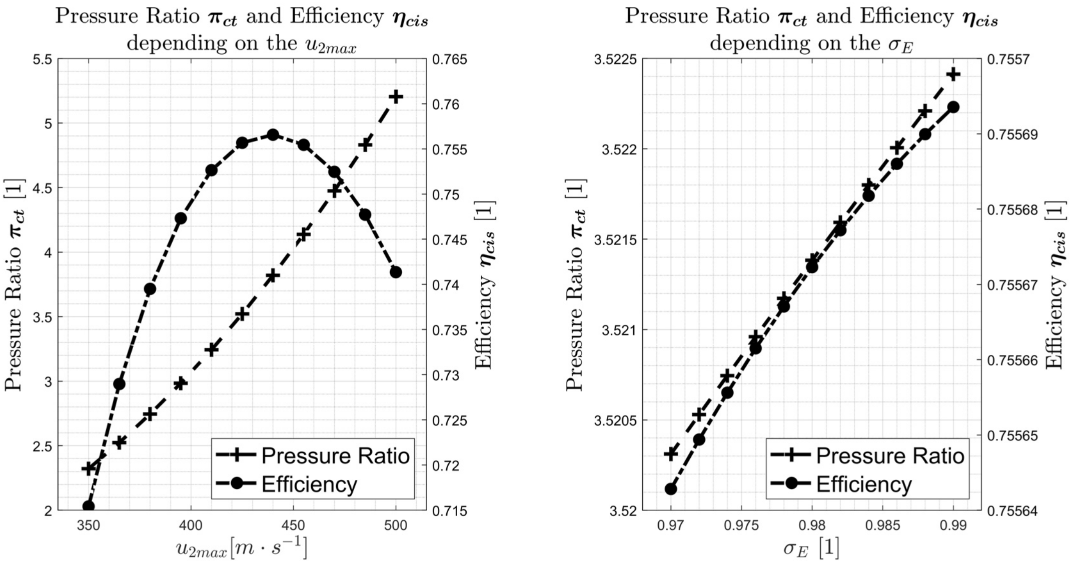

Fig. 5. Sensitivities of chosen parameters

Influence of individual parameters is assessed as the difference between its minimum and maximum value in the efficiency and pressure ratio. The summary of the influences can be seen in Fig. 6. If the difference is negligible, then the parameter is marked with the symbol '$\times$'.

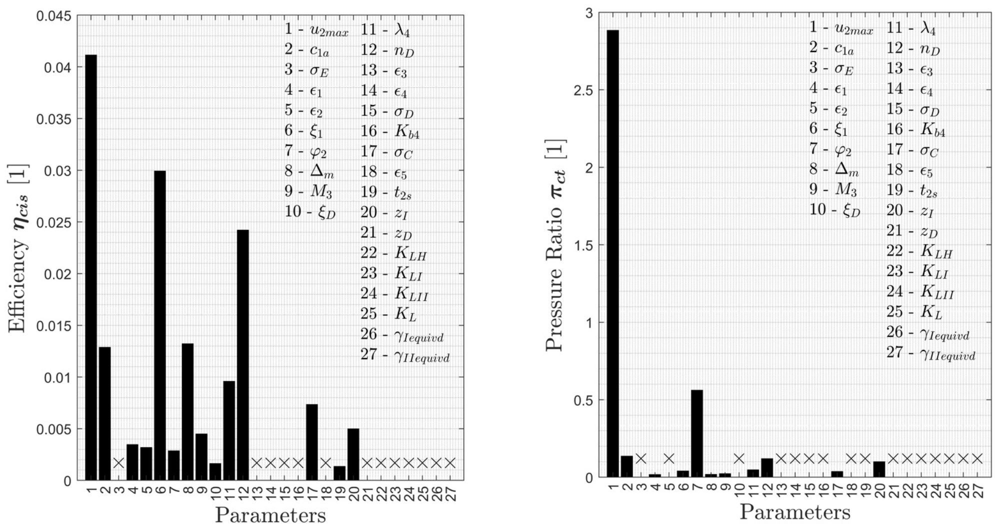

Fig. 6. Influence of individual parameters

Several parameters were selected to perform a more detailed sensitivity study. These parameters can make the difference in efficiency more than 0.5 % or they influence the resulting pressure ratio (with respect to the chosen span of values). We gain a set of nine parameters – $u_{2\max}$, φ_2, c_{1a}, ξ_i, n_D, δ_m, λ_4, σ_C and z_r (descending order of influence).

From the computed results, we will focus on the parameters δ_m and φ_2. In Fig. 7, it can be seen that as the radial clearance δ_m increases (in arrow direction), both efficiency and pressure ratio decrease. The increasing angle of impeller blades at the outlet φ_2 leads to higher efficiency and pressure ratio (Fig. 8). These results are in accordance with the knowledge in [4] and [7].

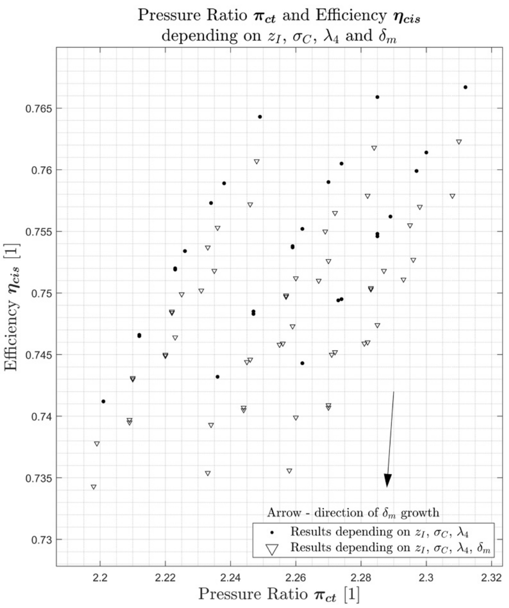

Fig. 7. Radial clearance

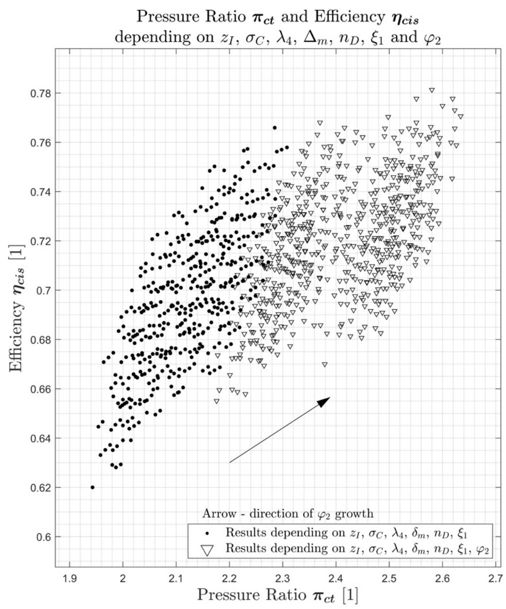

Fig. 8. Angle of impeller blades

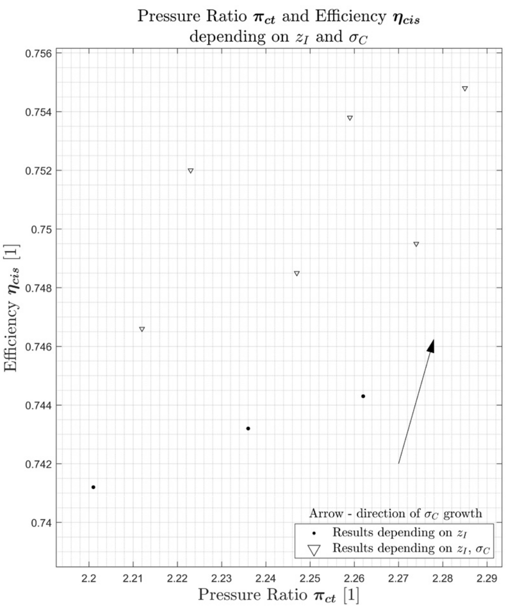

Fig. 9. Collector loss coefficient

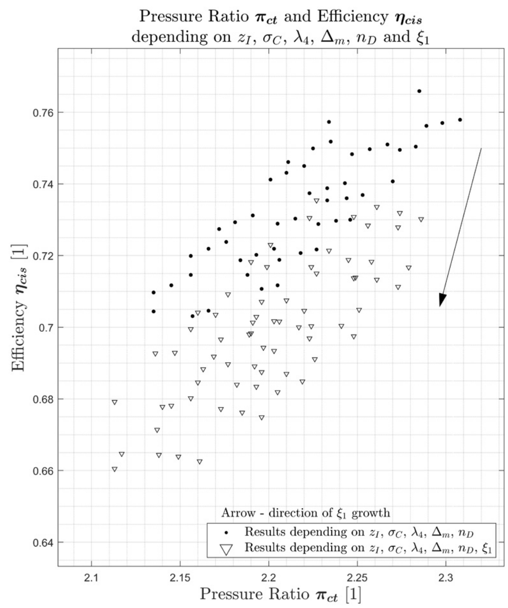

Fig. 10. Impeller loss

In Figs. 9 and 10, it can be seen that there are two other parameters that affect the efficiency and pressure ratio, as well. The parameter σ_C characterizes pressure loss in the collector. Its value depends on the design solution. Some authors state that this decrease is neglected for small compressors [18]. Since we consider the total pressure p_{5t} estimation at the collector as $p_{5t} = \sigma_C p_{4t}$, Fig. 9 shows that the difference in the isentropic efficiency can be up to 1 %.

The friction loss coefficient ξ_I quantifies the friction loss along the impeller. These losses include the disc friction loss, recirculation loss, blade loading loss, skin friction loss and incidence loss (when prewhirl is applied [11, 14]). These losses are thoroughly explained in [9]. Fig. 10 justifies the importance of choosing the coefficient as realistically as possible. The difference in isentropic efficiency for various ξ_I is up to 4 %.

In Fig. 11, there are results considering (and varying) all nine parameters that make the biggest difference in the compressor performance. Optimal set of inputs is indicated as the upper boundary curve constructed using the 4th order least squares method (LSM).

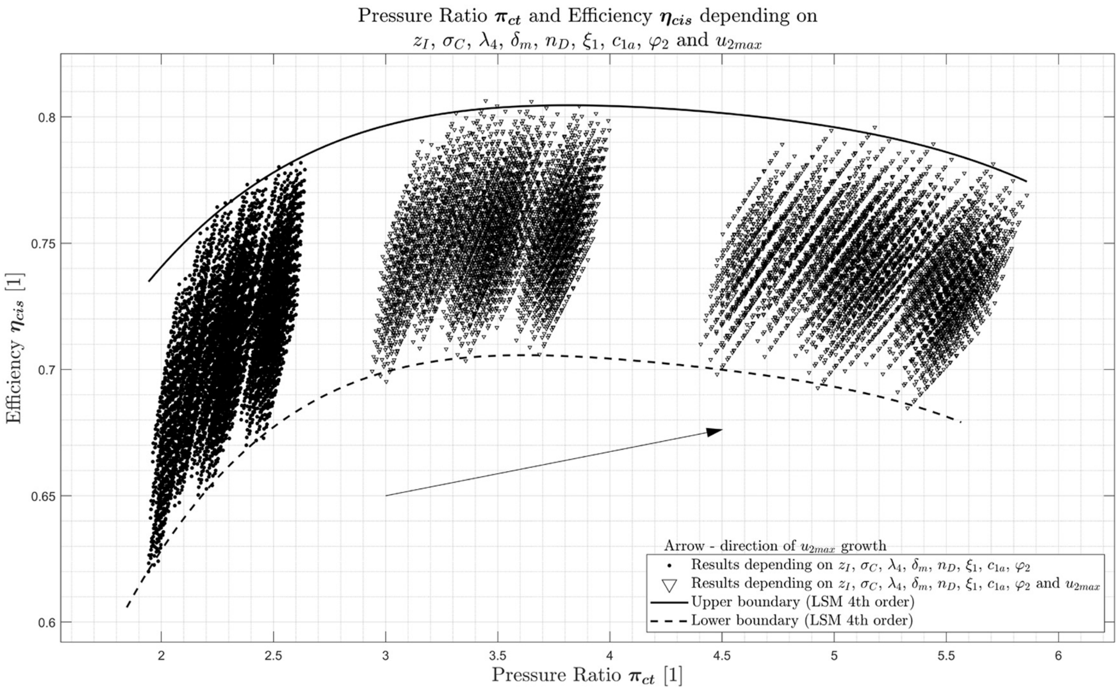

Fig. 11. Sensitivity study results

Not all cases lead to satisfying designs. On the other hand, there can be seen that isentropic efficiency can be higher than it was computed in the example case (described in [14]). With the appropriate choice of inputs, especially $u_{2\,\max}$, the isentropic efficiency η_{cis} could be higher than 80 %. Some notable results are summarized in Table 4. Furthermore, some cases lead to one-dimensional designs with 80 % in efficiency and value of pressure ratio up to 4.6.

Table 4. Results at the upper boundary curve

Top efficiency		Reached efficiency at design point		Top pressure ratio with 80 % efficiency	
η_{cis}	π_{ct}	η_{cis}	π_{ct}	η_{cis}	π_{cts}
80.8 %	3.96	80.4 %	4.19	80.0 %	4.59

5. Multi-criteria optimization

The optimization method for one-dimensional design of radial-flow compressor is presented in this section. Parametric study performed in Section 4 is taken into account.

One-dimensional radial-flow compressor design requires a significant amount of knowledge to determine the plausible values of various coefficients entering the design process. Many input parameters determine losses along the airflow channels. Including these loss coefficients into the optimization process clearly leads to their minimization. Parameters $\delta_m, \epsilon_1, \epsilon_2, \sigma_E, \xi_I, \xi_D, n_D, \epsilon_3, \epsilon_4, \sigma_D, \sigma_C$ and ϵ_5 are not included into optimization process. Loss coefficients need to be specified and are considered constant during optimization. Radial clearance δ_m between the impeller and shroud causes additional aerodynamic losses. Collector elbow radius coefficient K_{b4} needs to be as low as possible to minimize D_{5e}. These two parameters are excluded from parameter optimization as well.

Main design parameters (Q_v, n, D_{1i}, D_{5emax}, c_0, c_5, H) are given from the general engine design. Parameters defining the geometry of the impeller airflow channel (see Fig. 2) do not affect one-dimensional design. The geometry of the vane diffuser directly affects the external diameter D_{5e}. On the other hand, the parametric study conducted in the previous section proves that input parameters defining vane diffuser geometry (Fig. 3) can be excluded from the optimization process. Mean blade thickness at impeller outlet t_{2s} is also excluded based on Fig. 6. Finally, Laval number at vane diffuser outlet λ_4 is not included into optimization process since it's value has been always maximized for wide range of weighting coefficient combinations.

Fixed parameters with corresponding values[3] are ordered in Table 2. Optimization has been performed in Matlab using the fmincon function [12], which finds the minimum of the constrained nonlinear multi-variable function. The goal is to minimize the cost function CF by alternating the remaining input parameters z_I, z_D, $u_{2\,\max}$, c_{1a}, φ_2 ordered into a vector $\boldsymbol{p}$

$$\boldsymbol{p} = [z_I, z_D, u_2, c_{1a}, \varphi_2]. \tag{15}$$

Upper and lower bounds are defined for every parameter based on the recommended span as

$$\begin{aligned} \boldsymbol{lb} &= [25, 15, 380, 100, 45], \\ \boldsymbol{ub} &= [35, 35, 550, 150, 90]. \end{aligned}$$

5.1. Cost function

The goal of the optimization is to maximize both the pressure ratio π_{ct} and compressor isentropic efficiency η_{kis}. Furthermore, minimal dimensions, the especially outer diameter D_{5e} are desired. Finally, manufacturing costs are taken into account (u_2, z_I and z_D). Cost function CF is constructed as

$$CF = a_{\pi_{ct}} \left(\frac{1}{\pi_{ct}}\right)^2 + a_{\eta_{cis}} \left(\frac{1}{\eta_{cis}}\right)^2 + a_{D5e} D_{5e}^2 + a_{u2} u_2^2 + a_{zI} z_I + a_{zD} z_D, \tag{16}$$

where $a_{\pi_{ct}}$, $a_{\eta_{kis}}$, a_{D5e}, a_{zI}, a_{zD} and a_{u2}, are the weighting coefficients. First of all, weighting coefficients a_i were normed to ensure that ratios of individual terms in (16) change as much proportionally to their weighing coefficients[4] as possible. This has been performed for vector p_{mean} composed from mean values of individual parameters being optimized.

[3]These values are held constant for optimization purposes.

[4]Without this, term $a_{u2} u_2^2$ would increase CF massively if change of a_{u2} from 1 to 2 have been performed. On the other hand, same increase of $a_{\pi_{kc}}$ from 1 to 2 would cause much smaller growth of CF than in previous case.

5.2. Example

Several optimizations have been performed for the following cases:

1) maximization of total pressure ratio π_{ct},
2) maximization of isentropic efficiency η_{cis},
3) minimization of outer diameter D_{5e},
4) combination of cases 1), 2), 3),
5) $a_i = 1$ for all weighting coefficients.

Fixed parameters were set to values in Table 2. Remaining parameters were set to:

$$\epsilon_1 = \epsilon_2 = 0.98, \quad \epsilon_3 = \epsilon_4 = \epsilon_5 = 0.97, \quad t_{2s} = 3\,\mathrm{mm}.$$

Results of the performed optimizations are in Table 5. Number of impeller blades z_I and diffuser vanes z_D are rounded at the end of optimization. Optimization has been performed for different sets of initial conditions. When a given parameter does not affect the cost function CF, the symbol '$\times$' is used and the optimized parameter differ for individual initial conditions. Since the number of impeller blades and number of diffuser vanes cannot be precisely stated in certain cases, then some parameters vary, as well.

Table 5. Performed optimizations

Parameter	$a_{\pi_{ct}}$	$a_{\eta_{cis}}$	$a_{D_{5e}}$	a_{u_2}	a_{z_I}	a_{z_D}	$[n_I, n_D, u_2, c_{1a}, \varphi_2]$	π_{ct}	η_{cis}	D_{5e}
Case \Unit	[1]						$[1, 1, \mathrm{m\,s^{-1}}, \mathrm{m\,s^{-1}}, ^\circ]$	[1]	[1]	[m]
1)	1	0	0	0	0	0	$[35, \times, 550, 100, 90]$	7.22	0.718	–
2)	0	1	0	0	0	0	$[25, \times, 477, 100, 45]$	4.12	0.778	–
3)	0	0	1	0	0	0	$[35, 35, 380, 100, 45]$	2.41	0.734	0.672
4)	1	1	1	0	0	0	$[25, 35, 520, 100, 90]$	6.15	0.751	0.882
5)	1	1	1	1	1	1	$[25, 16, 470, 100, 90]$	4.80	0.771	0.946

Table 5 shows that the resulting pressure ratio π_{ct}, compressor isotropic efficiency η_{cis} and external diameter D_{5e} correspond with chosen weight coefficients. In the first case, when maximal pressure ratio is desired, we obtained the highest pressure ratio from all studied cases. However, efficiency was at it's minimum. When the highest possible efficiency was desired, resulting pressure ratio was significantly lowered. In the third case there were no requirements on neither π_{ct} or η_{cis}. The smallest external diameter was desired. Considering only spatial restriction leads to unacceptably low pressure ratio and compressor isotropic efficiency. When all three mentioned criteria are combined, we obtain compromise from former three cases.

6. Conclusion

The structure of the one-dimensional design algorithm for radial-flow compressor stage has been described. The presented algorithm was compared with the design method from [14]. This comparison affirms that all kinds of one-dimensional design algorithms differ mainly in aerodynamic loss model. The parametric study unveils which parameters have the most significant effect on the performance indicators of the radial compressor stage. There was shown that eighteen parameters from twenty-seven considered influence compressor design very little. Optimization tool was assembled based on the results of the parametric study. It confirmed that during the design process there is a lot of contradictory requirements. For instance, demanding a minimal compressor outer diameter leads to unsatisfactory performance indicators. Furthermore, combining both the requirements on performance parameters and compressor dimensions leads to compromise.

Further work will concern the calculation of spatial impeller blade geometry. After that, one-dimensional CFD simulation through the radial compressor stage will be performed. Subsequently, three-dimensional analysis of airflow inside the centrifugal compressor should be carried out. Finally, fully parametric tool for a complete centrifugal compressor design combining initial one-dimensional computation with complex three-dimensional flow analysis accompanied with optimization processes should be developed.

Acknowledgements

Authors acknowledge support from the ESIF, EU Operational Programme Research, Development and Education, and from the Center of Advanced Aerospace Technology (CZ.02.1.01/0.0/0.0/16 019/0000826), Faculty of Mechanical Engineering, Czech Technical University in Prague.

References

[1] Aungier, R. H., Centrifugal compressor stage preliminary aerodynamic design and component sizing, Turbo Expo: Power for Land, Sea, and Air, American Society of Mechanical Engineers, 1995. https://doi.org/10.1115/95-GT-078

[2] Aungier, R. H., Centrifugal compressors: A strategy for aerodynamic design and analysis, AMSE Press, New York, USA, 2000. https://doi.org/10.1115/1.800938

[3] Van den Braembussche, R., Design and analysis of centrifugal compressors, John Wiley & Sons, 2019. https://doi.org/10.1002/9781119424086

[4] Cumpsty, N. A., Compressor aerodynamics, Krieger Pub., Florida, 2004.

[5] Demeulenaere, A., Van den Braembussche, R., Three-dimensional inverse method for turbomachinery blading design, ASME 1996 International Gas Turbine and Aeroengine Congress and Exhibition, American Society of Mechanical Engineers Digital Collection, 1996, pp. 247–255. https://doi.org/10.1115/96-GT-039

[6] Eckert, B., Axial and radial compressors: Application/theory/calculation, Springer-Verlag, Berlin, 1953. (in German)

[7] Farokhi, S., Aircraft propulsion, John Wiley & Sons, 2014.

[8] Föző, L., et al., Mathematical modeling of radial compressor of a turbojet engine, IEEE International Conference on Computational Cybernetics (ICCC), 2009. https://doi.org/10.1109/ICCCYB.2009.5393936

[9] Gutiérrez Velásquez, E. I., Determination of a suitable set of loss models for centrifugal compressor performance prediction, Chinese Journal of Aeronautics 30 (5) (2017) 1644–1650. https://doi.org/10.1016/j.cja.2017.08.002

[10] Johnston, J. P., Dean, R. C., Losses in vaneless diffusers of centrifugal compressors and pumps: Analysis, experiment, and design, Journal of Engineering for Power 88 (1) (1966) 49–60. https://doi.org/10.1115/1.3678477

[11] Li, P., Design of a high pressure ratio centrifugal compressor, DEStech Transactions on Computer Science and Engineering (2018). https://doi.org/10.12783/dtcse/cmsam2018/26572

[12] MATLAB, 9.7.0.1190202 (r2019b), The MathWorks Inc.: Natick, MA, USA (2018).

[13] Nili-Ahmadabadi, M., Durali, M., Hajilouy-Benisi, A., A novel quasi 3-D design method for centrifugal compressor meridional plane, Turbo Expo: Power for Land, Sea, and Air, 2010, pp. 919–931. https://doi.org/10.1115/GT2010-23341

[14] Růžek, J., Kmoch, P., Theory of aircraft engines – part I: Compressors, turbines and combustion chambers, Brno, 1979. (in Czech)

[15] Schiff, J., A preliminary design tool for radial compressors, Master Thesis, Lund University, Sweden, 2013.

[16] Smith, D. J. L., Merryweather, H., The use of analytic surfaces for the design of centrifugal impellers by computer graphics, International Journal for Numerical Methods in Engineering 7 (2) (1973) 137–154. https://doi.org/10.1002/nme.1620070205

[17] Vaněk, V., Matoušek, O., Method to design a radial compressor stage, Technical report, Prague, 1986. (in Czech)

[18] Watson, N., Janota, M., Turbocharging: The internal combustion engine, Palgrave, London, 1982. https://doi.org/10.1007/978-1-349-04024-7

[19] Xu, C., Centrifugal compressor design considerations, Fluids Engineering Division Summer Meeting, 2006, pp. 217–225. https://doi.org/10.1115/FEDSM2006-98061

[20] Xu, C., Design experience and considerations for centrifugal compressor development, Proceedings of the Institution of Mechanical Engineers, Part G: Journal of Aerospace Engineering 221 (2) (2007) 273–287. https://doi.org/10.1243/09544100JAERO103

[21] Zurita-Ugalde, V., Gomez-Mancilla, J. C., Garcia-Cristiano, F., A simple method for geometry definition of radial compressors, International Journal of Turbo and Jet Engines 18 (1) (2001) 31–36. https://doi.org/10.1515/TJJ.2001.18.1.31